

Thermal Characterization of Electronic Packages Using a Three-Dimensional Fourier Series Solution

J. R. Culham

Associate Professor and Director,
Mem. ASME,

M. M. Yovanovich

Professor Emeritus
and Principal Scientific Advisor,
Fellow ASME,

Microelectronics Heat Transfer Laboratory,
Department of Mechanical Engineering,
University of Waterloo,
Waterloo, Canada

T. F. Lemczyk

Project Engineer,
Louisiana State University,
Baton Rouge, LA 70821

The need to accurately predict component junction temperatures on fully operational printed circuit boards can lead to complex and time consuming simulations if component details are to be adequately resolved. An analytical approach for characterizing electronic packages is presented, based on the steady-state solution of the Laplace equation for general rectangular geometries, where boundary conditions are uniformly specified over specific regions of the package. The basis of the solution is a general three-dimensional Fourier series solution which satisfies the conduction equation within each layer of the package. The application of boundary conditions at the fluid-solid, package-board and layer-layer interfaces provides a means for obtaining a unique analytical solution for complex IC packages. Comparisons are made with published experimental data for both a plastic quad flat package and a multichip module to demonstrate that an analytical approach can offer an accurate and efficient solution procedure for the thermal characterization of electronic packages. [S1043-7398(00)01403-1]

Introduction

The accurate prediction of component junction temperatures in electronic packages can lead to complex and time consuming simulations. Although analytical techniques can provide accurate and expedient solution methods, it is generally perceived that the complex geometries associated with microelectronic packaging do not lend themselves to analytical procedures. Many researchers have used finite Fourier transform techniques to solve the heat conduction problem in multilayer structures found in integrated circuits. The solution procedures are generally limited to two- and three-dimensional analyses in geometrically conforming laminates as shown in Fig. 1. Through the selective application of appropriate boundary conditions, the solution procedures for conforming laminated structures can be easily modified to include the nonconforming structures found in many electronic packages.

Gray [1] and Kokkas [2] present steady-state and transient solutions, based on Fourier and Laplace transform techniques, for determining temperatures in a three-dimensional multilayer substrate. Lemczyk et al. [3] use a Fourier series solution to solve the three-dimensional heat conduction problem in a multilayer printed circuit board. The analytical approach used in all of these procedures is discussed in Carslaw and Jaeger [4]. Albers [5] introduces a recursion technique for improving the solution efficiency of Fourier transform methods in both rectangular and cylindrical multilayered structures. While all of these solutions can predict temperature or heat flux for any point in a three-dimensional field they are restricted to simple, rectangular laminates which do not resemble the more complex geometries found in any of the package geometries shown in Fig. 2.

Since the primary role of an electronic package is to provide protection to the sensitive components on the surface of the integrated circuit, the IC is generally fully encapsulated within a plastic or ceramic structure. The IC or die is bonded to a leadframe, which provides electrical pinout connections and an excellent path for dissipating excess heat. While some packages, such as plastic,

dual inline packages, fully encase the IC in a plastic mold, others such as ceramic quad flat packs, have an internal cavity where the IC can be attached to either the lower or upper surface surrounding the cavity. Conventional analytical models based on Fourier transform methods do not conform well to these complex geometries, found in most electronic packages.

The purpose of this paper is to present a modeling procedure that uses finite Fourier transform methods to simulate heat transfer in many of the package geometries used in present day microelectronic applications. While the analyses can be detailed, a general overview of the governing equations, boundary conditions, and solution procedures will be presented. A full solution, including the equation development and the approach used to code the solution, is presented by Lemczyk et al. [6]. The basis of the solution is a general three-dimensional Fourier series solution which precisely satisfies the conduction equation within each layer of the package. The application of boundary conditions at fluid-solid, package-board and layer-layer interfaces provides a means for obtaining a unique analytical solution for complex IC packages.

It will be demonstrated by comparison to published experimental data that an analytical approach can offer an accurate and time efficient solution procedure for the thermal characterization of electronic packages.

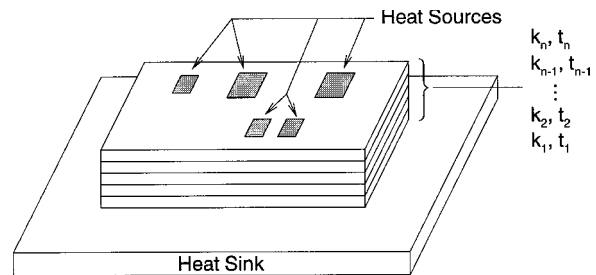


Fig. 1 Multiple layer substrate

Contributed by the Electrical and Electronic Packaging Division for publication in the JOURNAL OF ELECTRONIC PACKAGING. Associate Technical Editor: R. Wirtz.

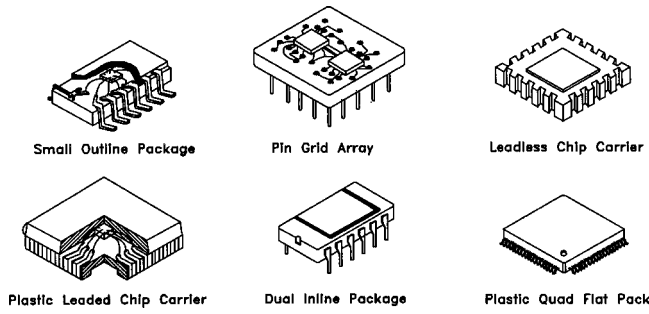


Fig. 2 Various package geometries reproduced from sketches in Bar-Cohen [11]

Modeling Procedure

Assumptions. Several assumptions have been used in the development of a thermal model for simulating microelectronic packages. Each of the assumptions is selected to simplify the mathematical calculations while preserving the physical integrity of the problem as much as possible.

The analysis is based on the solution to Laplace's equation, where heat is produced at the top surface of the die plane layer and there are no other sources of internal heat generation. The source of heat, typically a silicon wafer, is assumed to be infinitely thin with uniform heat generation.

The layers within the various sections of the package structure are assumed to be composed of homogeneous, isotropic materials of known thickness and thermal conductivity. This implies that layers, such as the lead frame, where the layer may consist of both a metallic frame and a plastic or ceramic binder, are considered to have a single value of thermal conductivity over the full extent of the layer.

Adjacent layers are assumed to be in perfect contact, where the contact resistance between layers is considered negligible and the temperature and the heat flux are equated across the interface.

The convective boundary conditions over the upper and lower surfaces of the package are assumed to be uniform. Each layer exposed along the sidewalls of the package can have a unique, uniformly specified convective boundary condition.

Single Layer Model. A basic three-dimensional rectangular, planar layer with a local coordinate reference is used to represent each layer. The overall length of the layer is L_1 and the overall width, L_2 as shown in the multilayer package in Fig. 3. The layer is assumed to have a homogeneous thermal conductivity k_i , and each exposed side face of the layer, numbered 1–4, has a uniquely specified boundary condition, denoted as $h_{j,i}$ and T_j where j refers to the particular side (1–4) and i refers to the layer number.

The controlling governing partial differential equation for three-dimensional steady state heat transfer in a rectangular, homogeneous body with no internal heat sources is Laplace's equation, given as

$$\frac{\partial^2 \theta}{\partial x^2} + \frac{\partial^2 \theta}{\partial y^2} + \frac{\partial^2 \theta}{\partial z^2} = 0 \quad (1)$$

where

$$\theta = T - T_a \quad (2)$$

and T_a is assumed to be a uniform ambient temperature which is specified for the four sides of each layer.

An exact, separable series solution for Eq. (1) can be written for the temperature rise within each layer as

$$\theta_i(x, y, z) = \sum_{m=1}^{\infty} \sum_{n=1}^{\infty} X_m(x) Y_n(y) Z_i(z) \quad (3)$$

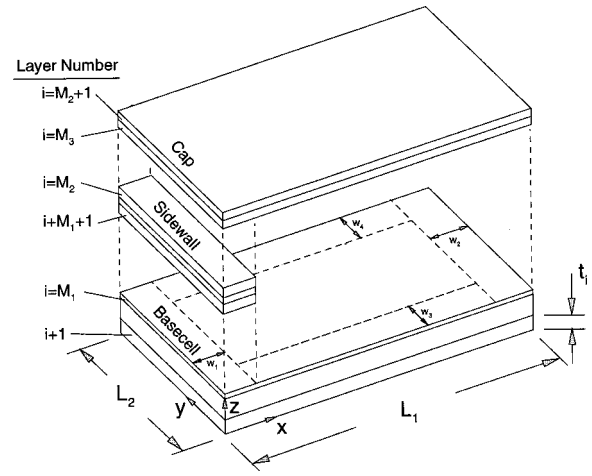


Fig. 3 Coordinate system for package model

For practical engineering purposes, the infinite series specified in terms of m and n in Eq. (3) are truncated to an upper limit N which can be arbitrarily specified subject to accuracy requirements and problem specific conditions. Typical values of m and n are in the range of 10–30, with an accuracy advantage obtained for higher values of the truncation limit along with a corresponding penalty in calculation time

$$\theta_i(x, y, z) = \sum_{m=1}^N \sum_{n=1}^N X_m(x) Y_n(y) Z_i(z) \quad (4)$$

The four sides of each layer are subject to a uniform, convective boundary condition, such that

$$L_1 \frac{\partial \theta_i}{\partial x} - \text{Bi}_{1,i} \theta_i = 0; \quad x = 0 \quad (5)$$

$$L_1 \frac{\partial \theta_i}{\partial x} + \text{Bi}_{2,i} \theta_i = 0; \quad x = L_1 \quad (6)$$

$$L_2 \frac{\partial \theta_i}{\partial y} - \text{Bi}_{3,i} \theta_i = 0; \quad y = 0 \quad (7)$$

$$L_2 \frac{\partial \theta_i}{\partial y} + \text{Bi}_{4,i} \theta_i = 0; \quad y = L_2 \quad (8)$$

where

$$\text{Bi}_{1,i} = \frac{h_{1,i} L_1}{k_i}; \quad \text{Bi}_{2,i} = \frac{h_{2,i} L_1}{k_i} \quad (9)$$

$$\text{Bi}_{3,i} = \frac{h_{3,i} L_2}{k_i}; \quad \text{Bi}_{4,i} = \frac{h_{4,i} L_2}{k_i}$$

The separation functions in Eq. (4), and the characteristic roots which automatically satisfy the boundary conditions in Eqs. (5)–(8) are defined as

$$X_m(x) = \cos(\epsilon_{m,i} x / L_1) + \frac{\text{Bi}_{1,i}}{\epsilon_{m,i}} \sin(\epsilon_{m,i} x / L_1) \quad (10)$$

$$Y_n(y) = \cos(\lambda_{n,i} y / L_2) + \frac{\text{Bi}_{3,i}}{\lambda_{n,i}} \sin(\lambda_{n,i} y / L_2) \quad (11)$$

$$Z_i(z) = a_{m,n}^{(i)} \cosh(\gamma_{m,n} z / L_1) + b_{m,n}^{(i)} \sinh(\gamma_{m,n} z / L_1) \quad (12)$$

$$\epsilon_{m,i}: (\epsilon_{m,i}^2 - \text{Bi}_{1,i} \text{Bi}_{2,i}) \sin(\epsilon_{m,i}) - \epsilon_{m,i} (\text{Bi}_{1,i} + \text{Bi}_{2,i}) \cos(\epsilon_{m,i}) = 0 \quad (13)$$

$$\lambda_{n,i}: (\lambda_{n,i}^2 - \text{Bi}_{3,i} \text{Bi}_{4,i}) \sin(\lambda_{n,i}) - \lambda_{n,i} (\text{Bi}_{3,i} + \text{Bi}_{4,i}) \cos(\lambda_{n,i}) = 0 \quad (14)$$

$$\gamma_{m,n}^{(i)} = \sqrt{\epsilon_{m,i}^2 + \left(\frac{L_1}{L_2} \lambda_{n,i}\right)^2} \quad (15)$$

The separation functions $X_i(x)$ and $Y_j(y)$ are determined based on layer geometry, properties and surface boundary conditions. The only remaining unknowns in the solution are the Fourier coefficients, $a_{m,n}^{(i)}$ and $b_{m,n}^{(i)}$, which can be determined based on the boundary conditions specified over the upper and lower planar surfaces. In the case of a multilayered structure, the Fourier coefficients in adjacent layers must be coupled in order to impress the influence of the boundary conditions at the upper and lower exposed surfaces throughout the multilayered structure.

A relationship between the two Fourier coefficients in a layer can be determined by using the uniformly specified boundary condition over the lower planar surface of that layer

$$L_1 \frac{\partial \theta_1}{\partial z} - \text{Bi}_{\text{bot}} (\theta_1 - \Theta_{\text{bot}}) = 0; \quad z = 0 \quad (16)$$

where

$$\text{Bi}_{\text{bot}} = \frac{h_{\text{bot}} L_1}{k_1} \quad (17)$$

$$\Theta_{\text{bot}} = T_{\text{bot}} - T_{s,1} \quad (18)$$

The boundary condition is applied over the full planar surface $0 \leq x \leq L_1$, $0 \leq y \leq L_2$. Since the boundary condition in Eq. (16) is uniform, the principle of orthogonality for the chosen Fourier series functions (which are themselves *orthogonal functions*) will directly result in a relationship between the Fourier coefficients in the layer.

$$b_{m,n}^{(1)} = f_{m,n}^{(1)} + g_{m,n}^{(1)} a_{m,n}^{(1)} \quad (19)$$

This directly relates $a_{m,n}^{(1)}$ to $b_{m,n}^{(1)}$ through the explicit constants $f_{m,n}^{(1)}$, $g_{m,n}^{(1)}$, where

$$f_{m,n}^{(1)} = \frac{-2(\text{Bi}_{\text{bot}} \Theta_{\text{bot}}) \sin(\epsilon_{m,1}) \sin(\lambda_{n,1})}{\gamma_{m,n}^{(1)} (\lambda_{n,1} + \sin(2\lambda_{n,1})/2) (\epsilon_{m,1} + \sin(2\epsilon_{m,1})/2)} \quad (20)$$

$$g_{m,n}^{(1)} = \frac{\text{Bi}_{\text{bot}}}{\gamma_{m,n}^{(1)}} \quad (21)$$

Multilayer Model. Each layer in a multilayered cell has a local coordinate system with a unique origin, which in turn conforms to the above specified equations. The numerical coupling of the governing equations within each layer is attained through the application of two boundary conditions along the common interface, based on the assumption of perfect contact between all adjacent layers. The two boundary conditions are specified such that temperature and heat flux are preserved across the interface at every point in the planar domain.

$$\theta_{i+1} = \theta_i + \Theta_i \quad (22)$$

$$\left. \frac{\partial \theta_{i+1}}{\partial z} \right|_{z=0} = \kappa_i \left. \frac{\partial \theta_i}{\partial z} \right|_{z=t_i} \quad (23)$$

where the relative difference between the specified ambient temperature in each layer, Θ_i , and the conductivity ratio, κ_i are given as

$$\Theta_i = T_{s,i} - T_{s,i+1} \quad (24)$$

$$\kappa_i = \frac{k_i}{k_{i+1}} \quad (25)$$

The interlayer boundary conditions in Eqs. (22) and (23) can be recast in terms of their Fourier series counterparts as

$$\sum_{m=1}^N \sum_{n=1}^N a_{m,n}^{(i+1)} X_{i+1} Y_{i+1} = \Theta_i \sum_{m=1}^N \sum_{n=1}^N \left(a_{m,n}^{(i)} \cosh\left(\gamma_{m,n}^{(i)} \frac{t_i}{L_1}\right) + b_{m,n}^{(i)} \sinh\left(\gamma_{m,n}^{(i)} \frac{t_i}{L_1}\right) \right) X_i Y_i \quad (26)$$

$$\sum_{m=1}^N \sum_{n=1}^N b_{m,n}^{(i+1)} \gamma_{m,n}^{(i+1)} X_{i+1} Y_{i+1} = \kappa_i \sum_{m=1}^N \sum_{n=1}^N \left(a_{m,n}^{(i)} \sinh\left(\gamma_{m,n}^{(i)} \frac{t_i}{L_1}\right) + b_{m,n}^{(i)} \cosh\left(\gamma_{m,n}^{(i)} \frac{t_i}{L_1}\right) \right) X_i Y_i \gamma_{m,n}^{(i)} \quad (27)$$

Equations (26), (27), and (19) provide the inter-layer relationships needed to determine the Fourier coefficients in each layer in terms of a single, unresolved Fourier coefficient, $a_{m,n}^{(1)}$.

Solution Procedure. For modeling purposes the electronic package, as shown in Fig. 3, has been divided into three distinct zones:

- (a) Basecell
- (b) Sidewalls
- (c) Cap

Each of these zones consists of one or more layers with the layer numbering scheme as indicated in Fig. 3. For the case of a fully encased package, the sidewall sections can be omitted, leaving a basecell and a package cap which sits directly on top of the die.

The temperature or heat flux solution for a multilayered substrate with either a single heat source, as shown in Fig. 4(a) or a multiple heat source configuration, as shown in Fig. 4(b), involves the solution of a mixed boundary value problem. The boundary conditions for each discrete section on the planar surface with the sources, referred to as the die plane layer, can be written as

$$L_1 \frac{\partial \theta_{M_1}}{\partial z} + \text{Bi}_j (\theta_{M_1} - \Theta_j) = \frac{q_j L_1}{k_{M_1}}; \quad z = t_{M_1} \quad (28)$$

where j denotes the section number and

$$\text{Bi}_j = \frac{h_j L_1}{k_{M_1}} \quad (29)$$

$$\Theta_j = T_j - T_{s,M_1} \quad (30)$$

The boundary condition over any section of the die plane layer can be fixed as either a convective condition through h_j , a temperature specified condition through T_j or a flux specified condition through q_j . Any combination of Bi_j , Θ_j , and q_j may be specified for each section and there may be an arbitrary combination and number of these sections. However, the total surface area of these sections *must* equal the total top surface area of the die plane shown in Fig. 4(a) or 4(b).

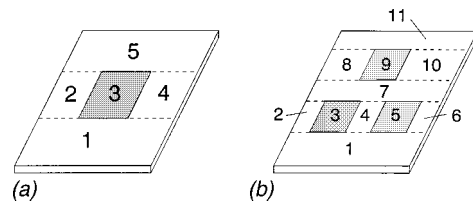


Fig. 4 Die plane control surfaces; (a) single source, (b) multiple sources

The sectional boundary condition in Eq. (28) can be applied to the Fourier series solution for the die plane layer allowing an approximation of the complete set of boundary conditions for each section of the form

$$\sqrt{\int (Au-f)^2} = \min \quad (31)$$

We note here that the generalized equation to be satisfied is of the form $Au=f$, with u_n containing the approximate solution to the problem, in our case the series containing the remaining $a_{m,n}^{(M_1)}$ Fourier coefficients. The necessary condition to satisfy Eq. (31), involves the satisfaction of the set of equations

$$\frac{\partial \|Au-f\|^2}{a_k} = 0 \quad (32)$$

which leads to a uniquely solvable solution, satisfying necessary and sufficient requirements of convergence and completeness. Utilizing the method of least-squares on the boundary (Kelman [7]) with respect to the coefficients $a_{m,n}^{(M_1)}$, a simple relationship can be obtained for the unresolved Fourier coefficient, $a_{m,n}^{(1)}$.

$$[A]a_{m,n}^{(1)} = r \quad (33)$$

Once $a_{m,n}^{(1)}$ is determined using a solution method such as Gaussian elimination, the complete set of Fourier coefficients can be determined which in turn allows temperatures to be calculated by substituting Eqs. (10)–(12) into Eq. (4).

Package Model. A quick comparison of the multiple layer stack shown in Fig. 1 and the cavity-up package shown in Fig. 5 reveals some similarities in geometry but many differences which must be considered if the Fourier series solution described above is to be used to model an electronic package.

Packages, such as fully encapsulated, dual inline packages, have a basecell section very similar to the multilayer stack shown in Fig. 1 but the die plane layer is encased with a layer of plastic or ceramic. The layer or layers above the die plane can be modeled exactly the same as the basecell section described previously. The cap of the package is a mirror image of the basecell, joined along the die plane layer using the assumption of perfect contact. As shown in Fig. 3, the layer numbering used in the cap is ordered from the top surface down to reflect the fact that it is a mirror image of the basecell section.

Substituting the appropriate Fourier series for the layers on either side of contacting interfaces into Eqs. (22) and (23) allows two equations to be obtained in terms of the Fourier coefficients at the die plane layer and the first layer in the basecell. For simplicity, E_1 , E_2 , E_3 , and E_4 are used to reflect the detailed terms

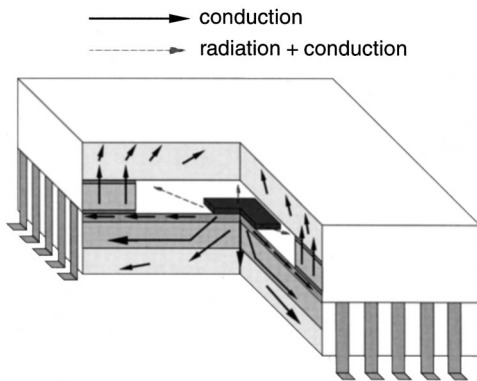


Fig. 5 Conductive and radiative heat transfer paths in an open cavity package

composed of geometric and thermophysical data resulting from these substitutions. The complete detailed evaluation is given in Lemczyk et al. [6].

$$E_1 a_{m,n}^{(M_1+1)} = E_2 a_{m,n}^{(1)} + d_1 \quad (34)$$

$$E_3 a_{m,n}^{(M_1+1)} = E_4 a_{m,n}^{(1)} + d_2 \quad (35)$$

Using the inter-layer relationships given in Eqs. (26) and (27), Eqs. (32) and (33) can be combined to form a single solution set in terms of $a_{m,n}^{(1)}$.

$$[A]a_{m,n}^{(1)} = r \quad (36)$$

where

$$A = E_3[E_1^{-1}E_2] - E_4 \quad (37)$$

$$r = d_2 - E_3(E_1^{-1}d_1) \quad (38)$$

The modeling of open cavity packages presents additional challenges because of the lack of one-to-one matching over the full extent of each adjacent layer and the addition of radiative heat transfer in the open cavity. Unlike the solution for the fully encapsulated package, the solution of the open cavity package requires the solution of a sectional or mixed boundary value problem along the interior face of the cap section. This mixed boundary condition allows for the perfect contact conditions over the sidewall section and the convective boundary (radiative+conductive heat transfer coefficient) over the exposed sections.

$$L_1 \frac{\partial \theta_{M_1}}{z} + \text{Bi}_{j,1}(\theta_{M_1} - \Theta_{j,1}) = \frac{q_{j,1}L_1}{k_{M_1}}; \quad z = t_{M_1} \quad (39)$$

$$L_1 \frac{\partial \theta_{M_3}}{z} + \text{Bi}_{j,3}(\theta_{M_3} - \Theta_{j,3}) = \frac{q_{j,3}L_1}{k_{M_3}}; \quad z = t_{M_3} \quad (40)$$

It should be clearly noted that unlike the user specified boundary conditions used in Eq. (16), these boundary conditions represent the thermal connection between the die plane and the cap layer through the interior cavity and the sidewalls. As a result the basecell and cap sections cannot be solved simultaneously. Instead, an iterative procedure is used to couple the two sections. The solution procedure in both the basecell and the cap sections is similar to that described previously.

The sidewall layers, adjoining the die plane and the cap layer, are modeled as one-dimensional fin sections in z .

$$\theta_{j,i} = a_{j,i} \cosh(\epsilon_{j,i}z) + b_{j,i} \sinh(\epsilon_{j,i}z); \quad \theta_{j,i} \equiv T_{j,i} - T_{s,i} \quad (41)$$

where for the sidewall sections the subscript j in Eq. (39) denotes the number of the side between 1 and 4.

The interior surface of each sidewall section is assumed to be insulated but the exposed outer surface has a user specified convective condition for each sidewall layer.

The fin solution coefficients can be uniquely determined from specified boundary conditions. Specifying the heat flux q_j and temperature for layer $M_1 + 1$ at $z=0$ (i.e., at the attachment to the die basecell), will give

$$a_{j,M_1+1} = \bar{T}_{j,M_1+1} - T_{s,M_1+1} \quad (42)$$

$$b_{j,M_1+1} = -q_{j,M_1+1} / (k_{M_1+1} \epsilon_{j,M_1+1}) \quad (43)$$

where

$$\epsilon_{1,i} = \sqrt{\text{Bi}_{1,i} / (L_1 w_1)}; \quad \text{Bi}_{1,i} = h_{1,i} L_1 / k_i \quad (44)$$

$$\epsilon_{2,i} = \sqrt{\text{Bi}_{2,i} / (L_1 w_2)}; \quad \text{Bi}_{2,i} = h_{2,i} L_1 / k_i \quad (45)$$

$$\epsilon_{3,i} = \sqrt{\text{Bi}_{3,i} / ((1 - (w_1 + w_2) / L_1) (L_2 w_3))}; \quad \text{Bi}_{3,i} = h_{3,i} L_2 / k_i \quad (46)$$

$$\epsilon_{4,i} = \sqrt{\text{Bi}_{4,i} / ((1 - (w_1 + w_2) / L_1) (L_2 w_4))}; \quad \text{Bi}_{4,i} = h_{4,i} L_2 / k_i \quad (47)$$

and w_j are the four sidewall widths, as shown in Fig. 3.

Combining Eqs. (40) and (41) with the perfect contact boundary condition between layers in the sidewalls allows all Fourier coefficients for the sidewalls to be calculated.

$$a_{j,i+1} = a_{j,i} \cosh(\epsilon_{j,i} t_i) + b_{j,i} \sinh(\epsilon_{j,i} t_i) + \Theta_i \quad (48)$$

$$b_{j,i+1} = \kappa_i \epsilon_{j,i} (a_{j,i} \sinh(\epsilon_{j,i} t_i) + b_{j,i} \cosh(\epsilon_{j,i} t_i)) / \epsilon_{j,i+1} \quad (49)$$

Using these coefficients, a heat flux from the sidewall and a mean temperature can be calculated, such that

$$T_{j,M_2} = a_{j,M_2} \cosh(\epsilon_{j,M_2} t_{M_2}) + b_{j,M_2} \sinh(\epsilon_{j,M_2} t_{M_2}) \quad (50)$$

$$q_{j,M_2} = -k_{M_2} \epsilon_{j,M_2} (a_{j,M_2} \sinh(\epsilon_{j,M_2} t_{M_2}) + b_{j,M_2} \cosh(\epsilon_{j,M_2} t_{M_2})) \quad (51)$$

The boundary condition over the exposed surface of the cap cell can be either flux specified, to represent a cavity down scenario or a convective condition to represent a cavity up arrangement with the radiative and conductive exchange in the cavity. The exchange of radiative heat transfer is assumed to be between the upper and lower planar surfaces of the cavity. The sidewalls are assumed adiabatic and do not absorb or emit heat.

The boundary conditions in the cavity are as follows:

Cavity-up

$$\frac{\partial \theta_{M_1}}{\partial z} + \frac{h_{\text{cav}}}{k_{M_1}} (\theta_{M_1} - \Theta_{\text{cap}}) = \frac{q_j}{k_{M_1}}; \quad z = t_{M_1} \quad (52)$$

$$\frac{\partial \theta_{M_3}}{\partial z} + \frac{h_{\text{cav}}}{k_{M_3}} (\theta_{M_3} - \Theta_{\text{die}}) = 0; \quad z = t_{M_3} \quad (53)$$

Cavity-down

$$\frac{\partial \theta_{M_1}}{\partial z} + \frac{h_{\text{cav}}}{k_{M_1}} (\theta_{M_1} - \Theta_{\text{cap}}) = 0; \quad z = t_{M_1} \quad (54)$$

$$\frac{\partial \theta_{M_3}}{\partial z} + \frac{h_{\text{cav}}}{k_{M_3}} (\theta_{M_3} - \Theta_{\text{die}}) = \frac{q_j}{k_{M_3}}; \quad z = t_{M_3} \quad (55)$$

where

$$\Theta_{\text{die}} = \bar{T}_{\text{die}} - T_{s,M_3} \quad (56)$$

$$\Theta_{\text{cap}} = \bar{T}_{\text{cap}} - T_{s,M_1} \quad (57)$$

The film coefficient in the cavity, h_{cav} is based on the radiative and conductive exchange between the two surfaces while convection is considered to be negligible.

$$h_{\text{cav}} = h_{\text{rad}} + h_{\text{cond}} \quad (58)$$

Model Comparison

Lasance et al. [9] designed a hypothetical validation chip module to be used as a benchmark in a study of thermal characterization of electronic packages using a commercially available numerical simulation code. The idealized package with overall dimensions of 30 mm × 30 mm dissipated 1 W over a die 3 mm × 3 mm and consisted of four homogeneous layers as shown in Fig. 6(a), where the dimensions and thermal conductivities are listed in Table 1.

The geometry of their idealized package was simple enough that Lasance et al. used a conventional Fourier series solution for stacked laminates to obtain the mean temperature of the heat source. Although Lasance's data do not provide a validation for the more complicated geometries found in most electronic packages, they do provide a convenient benchmark for the fundamental multilayer solution presented in this paper.

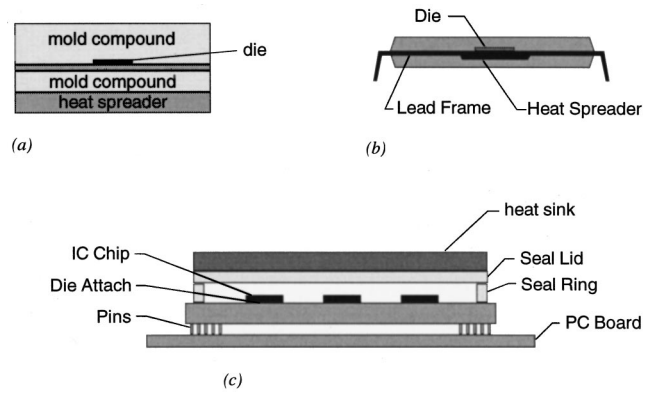


Fig. 6 Profiles of packages used for model validation; (a) validation chip module, (b) 208 pin plastic quad flat pack, (c) cavity up multichip module

Lasance et al. [9] do not discuss the details of their Fourier series model and as a result there may be minor differences between the Lasance model and the model presented herein. Even with the potential for some procedural differences, there is excellent agreement between the two models when calculating mean die temperature over a wide range of boundary conditions, as shown in Table 2.

Temmerman et al. [10] tested a 208 pin plastic quad flat pack using several different test procedures, including a submerged double jet impingement test where heat transfer coefficients in excess of $10^5 \text{ W}/(\text{m}^2 \cdot \text{K})$ can be obtained over the entire surface of the package. Other tests were performed using a cold plate on one or both planar surfaces of the package.

The plastic quad flat pack, as shown in Fig. 6(b), was constructed of plastic mold compound with outside dimensions of 28 mm × 28 mm, a thermal conductivity of 0.6 $\text{W}/(\text{m} \cdot \text{K})$ and an overall thickness of 3.6 mm. The plastic outer shell fully encapsulated a thermal test die (SGS-Thomson P655) that was 9.1 mm × 9.1 mm × 0.6 mm. The die was made of silicon with a reported thermal conductivity of 155 $\text{W}/(\text{m} \cdot \text{K})$. The test die was attached

Table 1 Geometric and thermophysical properties for the validation chip module

Layer	Thickness (mm)	Thermal Conductivity $\text{W}/(\text{m} \cdot \text{K})$
heat spreader	1.0	200.0
mold compound	1.0	0.2
lead frame	0.1	200.0
mold compound	2.0	0.2

Table 2 Comparison of junction temperatures between Lasance et al. [9] and current model

h ($\text{W}/(\text{m}^2 \cdot \text{K})$)				ΔT ($^{\circ}\text{C}$)		difference (%)
top	bot	side	lead	Lasance et al.	current model	
1	1	1	1	455.0	455.3	0.07
10	10	10	10	62.4	62.5	0.16
100	100	100	100	22.6	22.8	0.88
1000	1000	1000	1000	18.2	18.4	1.10
10^4	10^4	10^4	10^4	17.4	17.7	1.72
10^6	10^6	10^6	10^6	16.7	17.1	2.40
10^9	10^9	10^9	10^9	16.7	17.1	2.40
500	10	10	10	25.9	26.0	0.39
10	10	500	500	32.1	28.5	6.0
10	500	10	10	21.7	22.0	1.38
10^9	10^{-9}	10^{-9}	10^{-9}	25.4	25.5	0.39
10^{-9}	10^9	10^{-9}	10^{-9}	20.2	20.3	0.50
10^{-9}	10^{-9}	10^9	10^9	19.1	18.2	-4.71

Table 3 Comparison of junction to case resistance between Temmerman et al. [10] and the current model

Test	cold	cold	jet
	plate	plate	
h_{top} ($W/(m^2 \cdot K)$)	20	40	10^5
h_{bot} ($W/(m^2 \cdot K)$)	10^5	10^5	10^5
R_{jc} (exp.) ($^{\circ}C/W$)	10.19	10.19	7.30
R_{jc} (model) ($^{\circ}C/W$)	10.91	10.24	7.84
% difference	7.1	0.5	7.4

to a heat spreader with a thermal conductivity of 300 W/(m·K) and a thickness of 0.13 mm using a die attach material with a thermal conductivity of 2.5 W/(m·K) and a mean thickness of 0.005 mm. The heat spreader was then attached to the leadframe with 52 pins per side with a pitch of 0.5 mm. All testing was performed with a total power input of 1 W. Thermal resistance values were calculated based on measured values of the steady state power dissipation, the junction temperature and a reference temperature based on the cold plates, the fluid or the ambient conditions.

The difference between the experimental data and the Fourier series model is less than +7.5 percent for each of the three test procedures as shown in Table 3. No explanation is offered by Temmerman for the identical junction to case resistance when the heat transfer coefficient of the top surface changes from 20 to 40 W/(m²·K). The Fourier series model exhibits sensitivity to the change in the heat transfer coefficient and the resulting thermal resistance for the higher heat transfer coefficient is lower by 6.6 percent.

Sullhan et al. [8] examined several different types of packages, including pin grid arrays with single dies and multichip modules with five dies in both cavity up and cavity down configurations.

The cavity up multichip module (MCM) examined by Sullhan et al. [8] had a cross sectional profile as shown in Fig. 6(c). The substrate of the package consisted of a three layer stack, with the first layer made of alumina, the second was a leadframe layer made of kovar and finally a die attach layer of silver filled epoxy. For modeling purposes, the silicon dies were assumed to be infinitely thin with a uniform heat flux distribution. The seal ring or sidewalls of the MCM were designed to be a primary conductive path for heat dissipation to the aluminum heat sink attached to the seal lid of the package. The seal ring and seal lid were constructed from a copper tungsten alloy and molybdenum, respectively. The dimensions and the thermal conductivity of each of the materials used in the MCM are given in Table 4. Sullhan et al. [8] did not explicitly give the thermal resistance of their extruded aluminum

Table 4 Thicknesses and thermal conductivities used in the cavity up multichip module

Material	Thermal Conductivity ($m \cdot K$)	Thickness (mm)
Alumina	28.0	3.302
Kovar	15.57	1.270
Ag Epoxy	1.52	0.0762
C-W Alloy	159.0	1.778
Molybdenum	133.9	0.508
Thermal Grease	2.00	0.0762

Table 5 Data for dies in multichip modules

Die	Power (W)	Die Size ($mm \times mm$)	Die Centroid (x, y) (mm)	$T_j - T_a$ ($^{\circ}C$)	
				experiment	model
Die 1	2.23	11.35 × 10.72	(11.177, 35.641)	37	36.4
Die 2	3.35	11.51 × 10.72	(11.253, 12.741)	41	38.9
Die 3	3.35	8.33 × 7.37	(33.566, 39.033)	43	44.8
Die 4	1.535	8.56 × 6.86	(33.693, 26.299)	36	39.3
Die 5	1.535	8.56 × 6.86	(33.693, 8.829)	39	35.7

heat sink but representative values for $R_{\theta_{ja}}$ with an approach velocity of 1.5 m/s and a 50 mm × 50 mm × 12.5 mm heat sink are in the range of 2.1 to 2.8°C/W. For modeling purposes a value of $R_{\theta_{ja}} = 2.5^{\circ}C/W$ has been selected. A thermal grease was used between the heat sink and the seal lid to minimize the contact resistance and to promote heat transfer to the heat sink.

The MCM had 5 dies of various sizes and power levels as shown in Table 5. All exposed surfaces of the MCM are assumed to have a uniformly specified convective boundary condition. An approach velocity of 1.5 m/s (300 fpm) is used. The heat transfer coefficient is based on a formulation given by Sullhan et al., such that:

$$h = 2 \times 0.000546 \times \sqrt{V/L} \quad (59)$$

where V , the velocity is in fpm, the flow length, L is given in inches and the resulting heat transfer coefficient has units of W/(in.²·°C).

The MCM is attached to an FR-4 printed circuit board through the kovar leads. A lead conductance of 3400 W/(m²·K) was used for modeling based on a pin length of 4.57 mm (substrate+package standoff) and a pin conductivity of 15.57 W/(m·K).

The calculated die temperatures, as shown in Table 5, compare favorably with the measured die temperatures reported by Sullhan et al. The hottest die temperature differs from experimental measurements by 4.2 percent. Die 4 and die 5 are the same size and dissipate the same power. Normally one would expect die 5 to be the cooler of the two because it is located in the corner of the MCM and benefits from cooling to two adjoining sides. The model shows this trend; however, the experimental data show just the opposite.

Conclusions

The complex geometries found in most electronic package configurations can be modeled using analytical methods through the careful use of simplifying assumptions. The Fourier series solution presented here provides a method for calculating local temperature distributions, heat fluxes and thermal resistances with an accuracy of approximately ±5 percent using a fraction of the setup and simulation time expected with more traditional domain discretization procedures.

Acknowledgments

The authors acknowledge would like to acknowledge the financial support of the Materials and Manufacturing Ontario and R-Theta Inc., Mississauga, ON.

Nomenclature

- a, b = Fourier coefficients
- A = surface area of the body, m²
- A = coefficient matrix
- Bi = Biot number

f, g = explicit constants found in Eqs. (20) and (21)
 h = heat transfer coefficient, $W/(m^2 \cdot K)$
 i = layer identification
 j = die plane section identification
 k = thermal conductivity, $W/(m \cdot K)$
 L_1 = package length, m
 L_2 = package width, m
 M_1 = top layer in basecell (die plane layer)
 M_2 = top layer in sidewall sections
 M_3 = bottom layer in package cap
 N = series truncation limit
 t = layer thickness; m
 T = temperature; $^{\circ}C$
 u = solution vector
 x, y, z = Cartesian coordinates, m
 $X(x)$ = separation function
 $Y(y)$ = separation function
 $Z(z)$ = separation function
 w_j = sidewall widths, m

Subscripts

a = ambient
 bot = bottom surface
 cap = cap
 cav = cavity
 $cond$ = conduction
 die = die
 rad = radiation
 s = sidewall sections

Greek Symbols

ϵ = characteristic root for x -direction
 γ = composite characteristic root
 λ = characteristic root for x -direction

κ_i = conductivity ratio; $\equiv k_i/k_{i+1}$

θ = temperature rise, $^{\circ}C$

Θ = sidewall temperature difference as in Eqs. (18) and (24)

References

- [1] Gray, P. R., 1971, "Analysis of Electrothermal Integrated Circuits," IEEE J. Solid-State Circuits, **SC-6**, No. 1, pp. 8–14.
- [2] Kokkas, A. G., 1974, "Thermal Analysis of Multiple-Layer Structures," IEEE Trans. Electron Devices, **ED-21**, No. 11, pp. 674–681.
- [3] Lemczyk, T. F., Culham, J. R., and Yovanovich, M. M., 1989, "Analysis of Three-Dimensional Conjugate Heat Transfer Problems in Microelectronics," Numerical Methods in Thermal Problems, *Proceedings of the Sixth International Conference*, Swansea, U.K., pp. 1346–1356.
- [4] Carslaw, H. S., and Jaeger, J. C., 1959, *Conduction of Heat in Solids*, Second Edition, Oxford University Press, Oxford.
- [5] Albers, J., 1994, "An Exact Recursion Relation Solution for the Steady-State Surface Temperature of a General Multilayer Structure," *Proceedings of the 10th IEEE Semiconductor Thermal Measurement and Management Symposium*, Austin, TX, pp. 129–137.
- [6] Lemczyk, T. F., and Culham, J. R., 1992, "Thermal Analysis of Electronic Package Components," Microelectronics Heat Transfer Laboratory Report, UWM/HTL 9112 G-37, University of Waterloo, Waterloo, Canada, April, 1992.
- [7] Kelman, R. B., 1979, "Least Squares Fourier Series Solutions To Boundary Value Problems," SIAM Rev., **21**, No. 3.
- [8] Sullhan, R., Fredholm, M., Monaghan, T., Agarwall, A., and Kozarek, B., 1991, "Thermal Modeling and Analysis of Pin Grid Arrays and Multichip Modules," *Proceedings of the 7th IEEE Semiconductor Thermal Measurement and Management Symposium*, Phoenix, AZ, pp. 110–116.
- [9] Lasance, C., Vinke, H., Rosten, H., and Weiner, K., 1995, "A Novel Approach for the Thermal Characterization of Electronic Parts," *Proceedings of the Eleventh Annual IEEE Semiconductor Thermal Measurement and Management Symposium*, San Jose, CA, pp. 1–9.
- [10] Temmerman, W., Nelemans, W., Goossens, T., Lauwers, E., Lacaze, C., and Zemlianoy, P., 1995, "Validation of Thermal Models for Electronic Components," *Proceedings of the Technical Conference, International Electronics Packaging Conference*, San Diego, CA, pp. 142–150.
- [11] Bar-Cohen, A., 1994, "Trends in the Packaging of Computer Systems," *Cooling of Electronic Systems*, S. Kakac, H. Yuncu, and K. Hijikata, eds., *Series E: Applied Sciences*-Vol. 258, Kluwer Academic Publishers, Norwell, MA.